

# The Critical Number of Gold Atoms for a Metallic State Nanocluster: Resolving a Decades-Long Question

Meng Zhou, Xiangsha Du, He Wang,\* and Rongchao Jin\*



Cite This: *ACS Nano* 2021, 15, 13980–13992



Read Online

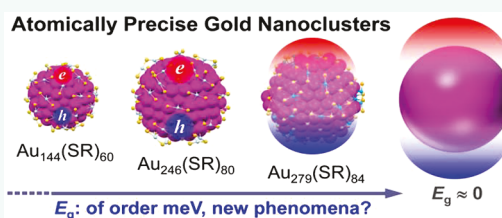
ACCESS |

Metrics & More

Article Recommendations

**ABSTRACT:** Probing the transition from a metallic state to a molecular state in gold nanoparticles is fundamentally important for understanding the origin of surface plasmon resonance and the nature of the metallic bond. Atomically precise gold nanoclusters are desired for probing such a transition based upon a series of precise sizes with X-ray structures. While the definition of the metallic state in nanoclusters is simple, that is, when the HOMO–LUMO gap ( $E_g$ ) becomes negligibly small ( $E_g < k_B T$ , where  $k_B$  is the Boltzmann constant and  $T$  the temperature), the experimental determination of ultrasmall  $E_g$  (e.g., of  $k_B T$  level) is difficult, and the thermal excitation of valence electrons apparently comes into play in ultrasmall  $E_g$  nanoclusters. Although a sharp transition from nonmetallic  $\text{Au}_{246}(\text{SR})_{80}$  to metallic  $\text{Au}_{279}(\text{SR})_{84}$  (SR: thiolate) has been observed, there is still uncertainty about the transition region. Here, we summarize several criteria on determining the metallic state *versus* the molecular (or nonmetallic) state in gold nanoclusters, including (1)  $E_g$  determined by optical and electrochemical methods, (2) steady-state absorption spectra, (3) cryogenic optical spectra, (4) transient absorption spectra, (5) excited-state lifetime and power dependence, and (6) coherent oscillations in ultrafast electron dynamics. We emphasize that multiple analyses should be performed and cross-checked in practice because no single criterion is definitive. We also review the photophysics of several gold nanoclusters with nascent surface plasmon resonance. These criteria are expected to deepen the understanding of the metallic to molecular state transition of gold and other metal nanoclusters and also promote the design of functional nanomaterials and their applications.

**KEYWORDS:** atomically precise gold nanoclusters, metal to nonmetal transition, surface plasmon resonance, electronic properties, excited-state dynamics, transient absorption, photophysics, coherent oscillations



Gold nanoparticles (Au NPs, typically 3–100 nm diameter) are well-known to exhibit surface plasmon resonance (SPR), which arises from collective excitation of conduction electrons.<sup>1</sup> Over the past two decades, the size- and shape-dependent SPRs of gold NPs have attracted wide research interest owing to their applications in nano-electronics, optics, photocatalysis, and biological sensing, to name a few.<sup>2–6</sup> These Au NPs show a quasi-continuous conduction band in their electronic structure, with an essentially zero gap ( $E_g \rightarrow 0$ ); that is, they are in a metallic state. Ultrasmall gold NPs (<2 nm in diameter), on the other hand, start to show discrete energy levels and accordingly multiple absorption peaks in the UV–vis spectra.<sup>7</sup> These ultrasmall NPs are often called nanoclusters (NCs), which exhibit optical properties being sensitive to the number of Au atoms and even the number of valence electrons because of strong quantum confinement effect.<sup>8</sup> In recent years, atomically precise Au NCs protected by thiolate (SR) ligands have been successfully synthesized, with each size possessing an

exact number of gold atoms and also of ligands, formulated as  $\text{Au}_n(\text{SR})_m$ , akin to molecules in organic chemistry. In addition, there has been tremendous progress in the atomic structure determination and applications of  $\text{Au}_n(\text{SR})_m$  NCs,<sup>8–20</sup> and it is now possible to synthesize and crystallize Au NCs up to hundreds of gold atoms per particle.<sup>9</sup> As the size of Au NCs increases, the energy levels of valence electrons will evolve into a quasi-continuous band and the Au NCs will become metallic.<sup>21</sup> Conventional colloid Au NPs are not truly monodisperse, and thus it was not possible to investigate the precise transition from a metallic to a nonmetallic state before

Received: June 2, 2021

Accepted: August 24, 2021

Published: September 7, 2021



the advent of atomically precise Au NCs. Therefore, structurally characterized Au NCs with atomic precision are desired for investigating the fundamental transition from molecular to metallic states.

Starting from the diatomic or few-atom clusters that possess large HOMO–LUMO gaps, the study on the transition from a molecular state to a metallic state with increasing size will help to reveal the origin of SPR and the metallic bonding, as well as the electronic screening and correlation interactions. The evolution of chemical and physical properties of Au NCs over such a transition has attracted wide interest from both experimental and theoretical researchers.<sup>22–28</sup> In the past decade, there have been several studies on the evolution from a molecular to a metallic state in Au NCs. In 2010, Goodson *et al.* combined several time-resolved spectroscopic methods to reveal that the critical size for the observation of quantum confinement is approximately 2.2 nm (~300 atoms estimated).<sup>29</sup> In 2012, Philip *et al.* investigated the nonlinear optical effects and determined that the Au NCs larger than Au<sub>144</sub> no longer show molecular-like behavior.<sup>30</sup> In 2015, Negishi *et al.* reported an experiment/theory combined study by which the nonmetal to metal transition should occur between Au<sub>144</sub> and Au<sub>187</sub>.<sup>31</sup> In 2016, Zhou *et al.* probed the electron relaxation dynamics of a series of Au NCs protected by the same type of ligand and concluded that the transition should occur between Au<sub>144</sub>(SR)<sub>60</sub> and Au<sub>333</sub>(SR)<sub>80</sub> NCs.<sup>21</sup> Similar conclusions were also reached by Kwak *et al.* using transient absorption and electrochemical methods in 2017.<sup>32</sup> Pettersson's group<sup>33</sup> and Knappenberger's group<sup>26</sup> reported that Au<sub>144</sub> was the smallest metallic-state gold NC by UV–vis and mid-IR pump–probe spectroscopy, respectively. There is still a debate on the Au<sub>144</sub> NC being in the metallic state or not,<sup>21,25,27,30</sup> which calls for further experimental and theoretical investigations. In 2017, electron dynamics and electrochemical methods proved that the giant 2.2 nm Au<sub>246</sub>(SR)<sub>80</sub> is still surprisingly nonmetallic.<sup>34</sup> In 2018, Higaki *et al.* discovered that the transition occurs sharply from Au<sub>246</sub>(SR)<sub>80</sub> (Au<sub>246</sub> for short hereafter) to Au<sub>279</sub>(SR)<sub>84</sub> (Au<sub>279</sub> for short hereafter) using low-temperature absorption and transient absorption spectroscopies.<sup>35</sup> Overall, it is nontrivial to determine whether a large size of NCs is in a metallic or nonmetallic state.

In this review, we discuss how to determine the transition from a nonmetallic to metallic state in Au NCs. Theoretically, when the HOMO–LUMO gap ( $E_g$ ) of NCs reaches  $E_g < k_B T$  (where  $k_B$  is the Boltzmann constant and  $T$  the temperature) with increasing size, the metallic state is formed (called the Kubo criterion), but experimentally how to determine ultrasmall  $E_g$  (*i.e.*, of meV or  $k_B T$  level) is by no means an easy task, and thermal excitation of valence electrons also comes into play in NCs with such ultrasmall  $E_g$ . In this article, we review several experimental criteria to determine the metallic *versus* the molecular state in Au NCs, including (1)  $E_g$  determination by optical absorption and electrochemical methods, (2) UV–vis–NIR (ultraviolet–visible–near-infrared) absorption spectroscopic features, (3) low-temperature absorption spectroscopic features, (4) transient absorption spectroscopic features, (5) excited-state lifetime and power dependence, and (6) coherent oscillations in transient absorption kinetics. Finally, we also review the photophysical properties of two Au<sub>*n*</sub> NCs with nascent SPRs and propose a method to estimate  $E_g$  (meV or  $k_B T$  level) from the excited-state lifetime. The above criteria and behaviors are important

for differentiating the Au NCs in the metallic state from those in the molecular state; the latter is synonymous with nonmetallic, semiconducting, or insulating (*i.e.*, large  $E_g$ ), all indicating an appreciable gap,  $E_g > k_B T$ . The obtained insights are expected to be useful in the future investigation of other metal NCs as well as alloy ones and to deepen the understanding of electronic screening and correlation effects and the nature of SPR and metallic bonding.

## CRITERIA FOR DETERMINATION OF THE MOLECULAR STATE AND METALLIC STATE

The overall current “roadmap” for the grand evolution is shown in Figure 1, where those sizes smaller than Au<sub>144</sub> are

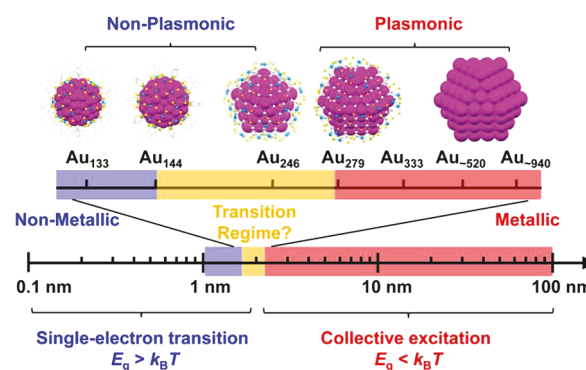


**Figure 1.** Schematic diagram of the grand transition from nonmetallic state ( $E_g > k_B T$ ) to metallic state ( $E_g < k_B T$ ) in Au NCs.

definitively molecular or nonmetallic (*i.e.*, with an appreciable, size-dependent  $E_g$ ), and those sizes larger than Au<sub>279</sub> (including Au<sub>279</sub> itself) are definitively metallic and plasmonic. The in-between sizes are intriguing, as some of them were reported to exhibit certain molecular<sup>36</sup> and metallic features (*e.g.*, in nonlinear optics<sup>25,30</sup> or ultrafast electron dynamics<sup>27</sup>), and there are still controversies in the literature. These aspects indeed motivated our current discussions on how to probe the molecular- to metallic-state transition, which is by no means an easy task and requires multiple analyses rather than any single analysis.

**$E_g$  Determination by Optical Absorption and Electrochemical Methods.** Metallic-state gold NPs exhibit a quasi-continuous conduction band, and there is no appreciable band gap, whereas molecular-state gold NCs show discrete energy levels and a size-dependent  $E_g$ . Therefore, the presence of  $E_g$  or not determines if a nanocluster is in the molecular or metallic state; note that the ultrasmall  $E_g$  (*e.g.*, meV or  $k_B T$  level) remains an intriguing issue and calls for future efforts in elucidation and precise measurements.

The relatively large  $E_g$  (*e.g.*, few eV down to ~0.5 eV) of Au NCs can be conveniently determined by their optical absorption. In small Au NCs (<2.2 nm core diameter), multiple absorption peaks can be observed in the steady-state UV–vis–NIR absorption spectra, which arise from single-electron transitions.<sup>36</sup> The  $E_g$  of small Au NCs (<~50 gold atoms in the core) can be easily determined by extrapolating the absorbance to zero (Figure 2A). We note that the HOMO–LUMO transition in gold NCs is typically dipole-allowed, thus, the optical gap is equal to the  $E_g$ , but the doped NCs often become more complicated, and many bimetallic cases were reported to show dipole-forbidden HOMO–

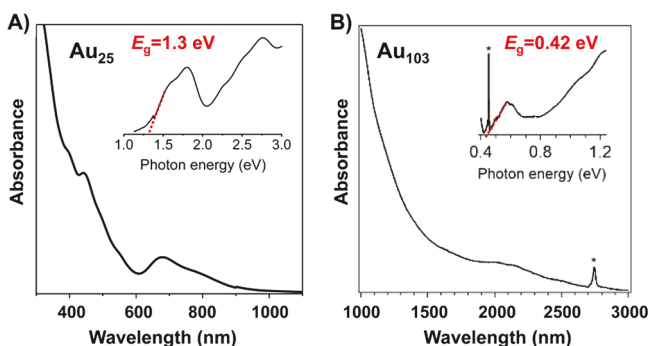


Figure 2. (A) UV-vis absorption spectrum of  $[\text{Au}_{25}(\text{SR})_{18}]^-$ . Reproduced from ref 43. Copyright 2018 American Chemical Society. (B) NIR absorption spectrum of  $\text{Au}_{103}\text{S}_2(\text{S-Nap})_{41}$ ; the asterisk (\*) indicates the solvent overtone vibrational absorption peak. Reprinted from ref 38. Copyright 2017 American Chemical Society. Both insets show the absorption spectra on the photon energy scale.

LUMO transitions.<sup>37</sup> As the size increases ( $\sim 50$ – $100$  gold atoms), the onset of the lowest-energy absorption peak will shift to longer wavelength as the  $E_g$  generally decreases with increasing size, although local zigzag behavior is observed (especially in  $n < 100$ ). With UV-vis-NIR absorption spectroscopy, we have been able to measure  $E_g$  as small as  $\sim 0.4$  eV.<sup>36,38</sup> For Au NCs with more than  $\sim 100$  Au atoms, their UV-vis absorption spectra show weaker and broader absorption bands in the NIR wavelength region (Figure 2B),<sup>39–41</sup> thus it becomes less possible to clearly resolve HOMO–LUMO gaps smaller than  $\sim 0.5$  eV. In the NIR

region, the solvent and surface ligand overtone signals appear (e.g., the asterisk in Figure 2B) and interfere with the  $E_g$  measurements when many overtone peaks are present in the  $E_g$  region.<sup>36,42</sup> When the size further increases, the NIR and IR absorption bands fade out and the spectrum retreats from the long wavelengths to the visible range,<sup>38</sup> and eventually, the SPR peak arises from collective excitation of electrons, which marks the negligible  $E_g$  and the emergence of the metallic state.

For large-sized Au NCs ( $>100$  gold atoms or so), the onset of steady-state optical absorption falls in the infrared region (wavelength  $>3000$  nm) and the absorption peaks become very weak and broadened. Therefore, it requires additional methods to determine the  $E_g$  of Au NCs. Electrochemical methods have been introduced as an effective tool for determining the  $E_g$  of gold and alloy nanoclusters.<sup>44</sup> We note that the optical method is subject to the dipole selection rule, but electrochemical charging is not, which means that the electron injection into a particle always fills the LUMO first and the hole injection (or oxidation) is always associated with the HOMO. Nevertheless, the electrochemical measurements are limited by the solvent and electrolyte “window” as well as the stability of charge states of NCs.

Generally, for Au NPs with different sizes, three voltammetric regimes were reported: bulk continuum, quantized double layer charging, and molecular-like.<sup>32,44</sup> The change of electrochemical potential of NPs between different redox state ( $\Delta V$ ) can be expressed by the following equation:<sup>44</sup>

$$\Delta V = ze/C_{\text{CLU}} \quad (1)$$

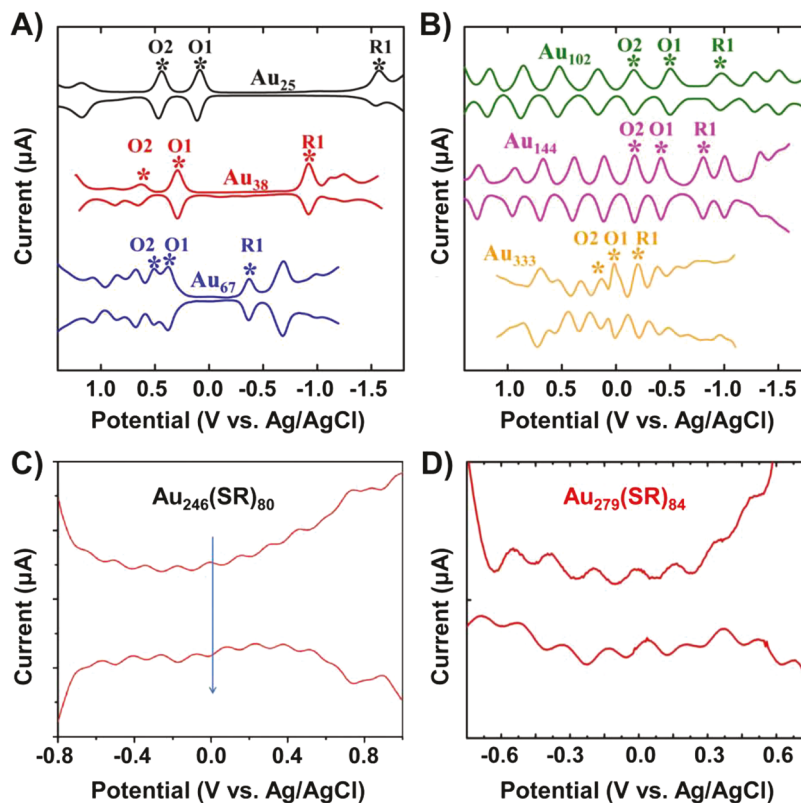


Figure 3. SWVs of (A)  $\text{Au}_{25}$ ,  $\text{Au}_{38}$ , and  $\text{Au}_{67}$  NCs and (B)  $\text{Au}_{102}$ ,  $\text{Au}_{144}$ , and  $\text{Au}_{333}$  NCs. Reproduced from ref 32. Copyright 2017 American Chemical Society. (C) SWV of  $\text{Au}_{246}(\text{SR})_{80}$  (the arrow indicates the open circuit potential, +0.01 V). Reprinted with permission from ref 34. Copyright 2017 Wiley-VCH. (D) DPV of  $\text{Au}_{279}$ . Reprinted from ref 50. Copyright 2018 American Chemical Society.

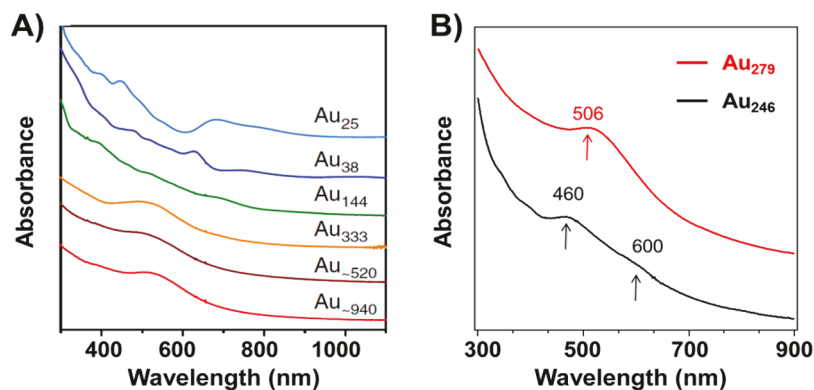


Figure 4. (A) UV-vis absorption spectra of a series of  $Au_n$  NCs. Reprinted with permission under a Creative Commons License from ref 21. Copyright 2016 Springer Nature. (B) Comparison of UV-vis absorption spectra between  $Au_{279}(SR)_{84}$  and  $Au_{246}(SR)_{80}$ . Reprinted from ref 35. Copyright 2018 American Chemical Society.

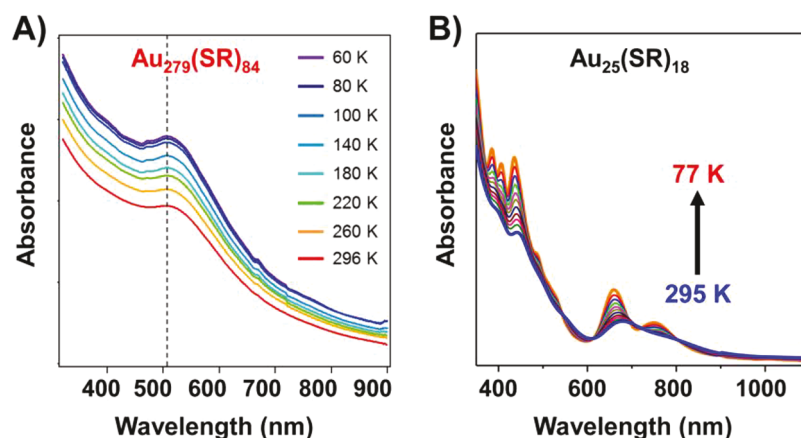


Figure 5. (A) UV-vis absorption spectra of  $Au_{279}(SR)_{84}$  at different temperatures. Reprinted from ref 35. Copyright 2018 American Chemical Society. (B) UV-vis absorption spectra of  $[Au_{25}(SR)_{18}]^-$  at different temperatures. Reproduced from ref 43. Copyright 2018 American Chemical Society.

where  $z$  is the charge of the NP,  $e$  is the elementary charge of the electron, and  $C_{CLU}$  is the capacitance of the NP. When  $\Delta V \ll k_B T$  (e.g., room temperature thermal energy, 25.7 meV), electron transfer from/to the NP will give rise to continuous charging *versus* the potential, and the NP is metallic. When  $\Delta V$  is slightly higher or comparable to  $k_B T$ , quantized double layer (QDL) charging can be observed in NPs, while their HOMO-LUMO gaps are difficult to resolve. When in the case of  $\Delta V \gg k_B T$ , significant potential spacing can be observed between the first reduction and first oxidation peaks, and the  $E_g$  can be estimated based on the electrochemical gap.

Both differential pulse voltammetry (DPV) and square wave voltammograms (SWV) have been used to investigate the electronic structures of Au NCs.<sup>38,45–47</sup> By subtracting the charging energy (potential spacing between successive oxidation or QDL peaks) from the electrochemical gap, one can estimate the HOMO-LUMO gap of a Au NC. In 2017, Kwak *et al.* investigated the electrochemical properties of six Au NCs ( $Au_{25}$ ,  $Au_{38}$ ,  $Au_{67}$ ,  $Au_{102}$ ,  $Au_{144}$ , and  $Au_{333}$ ) using the SWV method.<sup>32</sup> From Figure 3A, one can observe significant gaps between the first oxidation (O1) peak and reduction peak (R1) of  $Au_{25}$  (1.66 V), the  $E_g$  was determined to be 1.32 eV after subtracting the charging energy, and similarly,  $E_g = 0.99$  eV for  $Au_{38}$  and  $E_g = 0.5$  eV for  $Au_{67}$ . As the size increases, the O1–R1 gap decreases accordingly (Figure 3B); the electrochemical gap is 0.39 V for  $Au_{144}$  and 0.22 V for  $Au_{333}$ , which

approaches the charging energy (spacing between QDL peaks). While the  $E_g$  of  $Au_{144}$  was possible to determine ( $\sim 0.17$  eV), the larger Au NCs start to show almost evenly spaced current peaks; thus, accurate  $E_g$  below 0.1 eV is not easy to determine.<sup>48,49</sup> Similar behavior was also observed for  $Au_{246}$  and  $Au_{279}$ ,<sup>34,50</sup> both showing evenly spaced current peaks (Figure 3C,D), and it is not possible to estimate their  $E_g$ .

Therefore, electrochemical methods can be used to determine the  $E_g$  down to  $\sim 0.1$  eV reliably. For those molecular-like Au NCs, a significant gap can be observed between the O1 and R1 peaks. For those very large metallic Au NPs ( $>3$  nm), there is no peaks in SWV or DPV, and thus  $E_g \rightarrow 0$ . For those sizes in the transition regime with QDL features ( $\sim 150$ – $300$  gold atoms),<sup>47</sup> one will observe almost evenly spaced peaks, and thus, it is difficult to determine if they are in the metallic state or not, and additional characterization methods are needed.

**UV-Vis-NIR Absorption Spectra: Multiple Peaks versus Single Peak.** When the HOMO-LUMO gap is smaller than 0.1–0.2 eV, it becomes challenging to directly determine the  $E_g$  of Au NCs. Therefore, it calls for indirect methods to probe the NCs. As previously discussed, nonmetallic Au NCs show multiple absorption peaks while metallic-state Au NCs exhibit a single SPR absorption peak. In 2016, Zhou *et al.* investigated the optical properties of a series of Au NCs ( $Au_{25}$ ,  $Au_{38}$ ,  $Au_{144}$ ,  $Au_{333}$ ,  $Au_{520}$ , and  $Au_{940}$ ) with

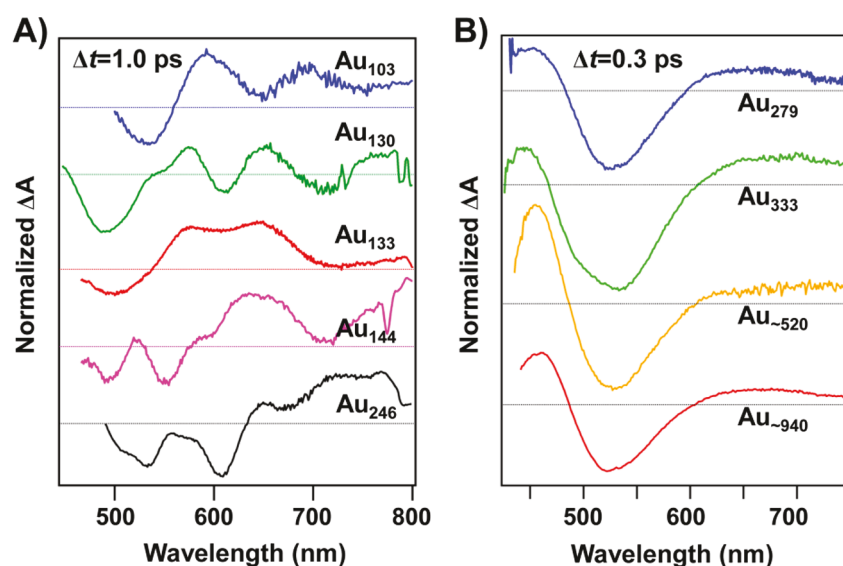


Figure 6. (A) TA spectra measured at 1 ps of a series of molecular-state Au NCs. (B) TA spectra measured at 0.3 ps of a series of metallic-state Au NCs. Both panels are reprinted from ref 36. Copyright 2019 American Chemical Society.

sizes spanning from 1.0 to 3 nm (see Figure 4A).<sup>21</sup> Au NCs smaller than Au<sub>144</sub> and the Au<sub>144</sub> itself show multiple absorption peaks, and those larger than Au<sub>333</sub> (including Au<sub>333</sub>) exhibit a single SPR absorption peak, which indicates that the transition from the metallic to the molecular state should occur between Au<sub>333</sub> and Au<sub>144</sub>. Subsequently Zeng *et al.* succeeded in the synthesis of Au<sub>246</sub>(SR)<sub>80</sub> and its structure determination.<sup>9</sup> Despite the large size of Au<sub>246</sub>(SR)<sub>80</sub>, it was identified to be nonmetallic by spectroscopic analyses.<sup>34</sup> In 2018, Higaki *et al.* further compared the optical properties between Au<sub>246</sub>(SR)<sub>80</sub> and Au<sub>279</sub>(SR)<sub>84</sub> and observed that Au<sub>279</sub> shows a single SPR absorption at 506 nm, whereas Au<sub>246</sub> exhibits multiple absorption peaks (Figure 4B);<sup>35</sup> note that the SPR of Au<sub>279</sub> was also reported by Sakthivel *et al.*<sup>50</sup> Although the two NCs of Au<sub>246</sub> and Au<sub>279</sub> have a similar size (2.2 nm, quasi-spherical) and similar electrochemical properties, the presence of SPR in Au<sub>279</sub> but not in Au<sub>246</sub> indicates the different nature in electronic excitation of the two NCs. Therefore, the presence of SPR peak is one of the criteria to determine the metallicity of Au NCs.

**Cryogenic Optical Spectroscopy: Sharpening and Shifting of Absorption Peaks or Not.** In addition to steady-state absorption at room temperature, cryogenic optical absorption spectra also show different features for metallic and molecular-state Au NCs. In metallic Au NPs and NCs, their SPR absorption does not show any change in the position and peak width at cryogenic temperatures compared to the features at room temperature (see Figure 5A).<sup>35</sup> In molecular-state Au NCs, however, UV–vis absorption peaks are sharpened and blue-shifted at lower temperatures (Figure 5B).<sup>43,51</sup> The different temperature dependences of UV–vis absorption for metallic and nonmetallic Au NPs arise from their different excitation mechanisms. In metallic gold NPs and NCs, photoexcitation gives rise to collective excitation of conduction electrons, and the dephasing mechanism is electron–electron interactions.<sup>52</sup> Therefore, a change in temperature will not significantly impact the SPR peak width and position. In molecular-like gold NCs, photoexcitation gives rise to a single-electron transition, and higher vibrational states will be excited thermally to couple with the electronic state. A significant

electron–phonon coupling (e–p coupling) is therefore involved in the absorption spectra of molecular-like gold NCs, and such an effect becomes more prominent for those ultrasmall sizes.<sup>51,52</sup> As a result, one can observe much more significant temperature dependence in UV–vis absorption spectra for ultrasmall gold NCs (see Figure 5B) as the thermal vibrations (or phonons) of the metal core are significantly reduced at lower temperatures. Therefore, by looking into the temperature-dependent UV–vis–NIR absorption spectra, it is also possible to differentiate molecular and metallic Au NCs.

**Transient Absorption Spectra: Single Peak versus Multiple Peaks.** Compared to the steady-state spectroscopy, time-resolved spectroscopy provides additional information on the electronic structure as well as the dynamics of photoexcited states. Time-resolved transient absorption spectroscopy (TAS) is a powerful tool to probe the excited-state dynamics of many materials, including metal NCs.<sup>53–55</sup> Since TAS measures the absorption difference between the excited state and the ground state at different time delays,<sup>21,24,26–28</sup> it does not require the sample to be luminescent. Therefore, TAS is an ideal method to investigate the excited states of gold NCs since most of them are only weakly luminescent.<sup>46–49</sup> In the TA spectra (difference in optical density ( $\Delta OD$ ) vs wavelength), the positive signal represents the excited-state absorption (ESA) and the negative signal is the ground-state bleaching (GSB) or stimulated emission (SE).

In molecular-state Au NCs, steady-state absorption spectra exhibit multiple absorption peaks. Similarly, one should observe several GSB peaks in the TA spectra, which arise from the bleaching of the ground-state absorption (Figure 6A).<sup>56</sup> Moreover, one would observe significant and broad ESA bands in the TA spectra of molecular-state Au NCs.<sup>11,50</sup> Those intense ESA bands should originate from the discrete energy levels in Au NCs. In metallic-state Au NCs and NPs, on the other hand, UV–vis absorption spectra are dominated by SPR. In the TA spectra, one would observe a strong GSB that arises from the SPR absorption and two ESA wings on the left and right sides of the GSB (Figure 6B, where the gray horizontal lines represent the baselines).<sup>36</sup>

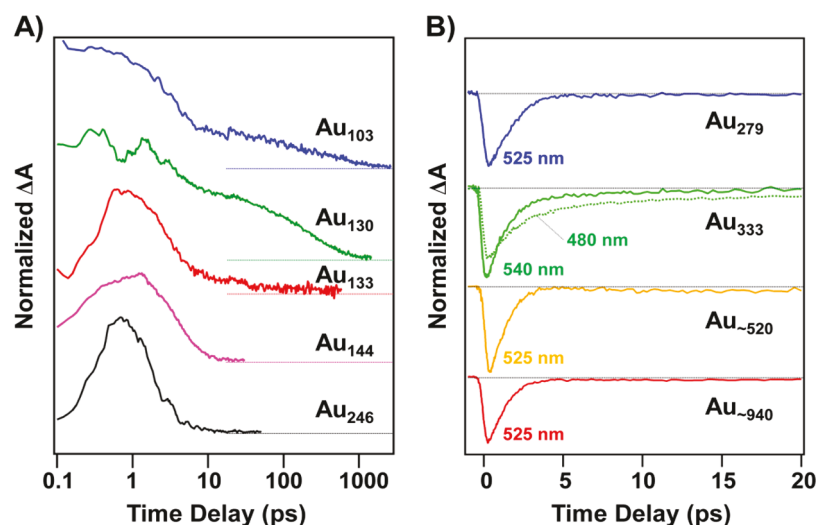


Figure 7. TA kinetics of a series of (A) nonmetallic Au NCs and (B) metallic Au NCs. Both panels are reprinted from ref 36. Copyright 2019 American Chemical Society.

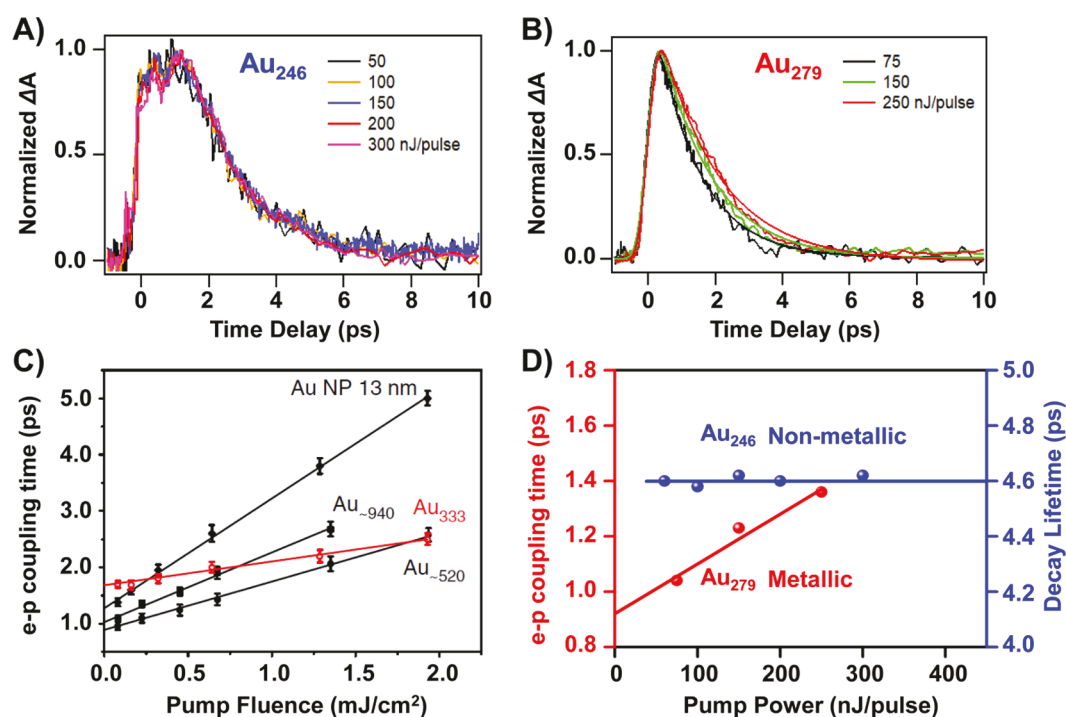


Figure 8. (A) TA kinetic traces of  $\text{Au}_{246}$  under different pump power. Reproduced with permission from ref 34. Copyright 2017 Wiley-VCH. (B) TA kinetic traces of  $\text{Au}_{279}$  under different pump power. Reproduced from ref 35. Copyright 2018 American Chemical Society. (C) Electron-phonon coupling times of different sized Au NCs with different pump fluences. Reprinted with permission under a Creative Commons License from ref 21. Copyright 2016 Springer Nature. (D) Relaxation lifetimes of  $\text{Au}_{246}$  and  $\text{Au}_{279}$  under various pump power. Reprinted from ref 35. Copyright 2018 American Chemical Society.

In time-resolved absorption spectra, the GSB peaks in both molecular-like and metallic Au NCs are sharpened and hence easier to identify than in the steady-state absorption spectra. For example, at first glance, the  $\text{Au}_{246}$  steady-state absorption spectrum appears metallic owing to the seemingly single pronounced peak at 460 nm, whereas the 600 nm peak is faint (Figure 4B); however, femtosecond transient spectra clearly revealed multiple GSB peaks,<sup>34</sup> hence, nonmetallicity in  $\text{Au}_{246}$ , albeit no distinct  $E_g$  was found (*i.e.*, below the detection limit) in SWV analysis on  $\text{Au}_{246}$ .<sup>34</sup> This example illustrates the

importance of multiple analyses rather than any single analysis such as electrochemistry.

Overall, multiple GSB peaks together with intense ESA bands can be observed in molecular-state Au NCs, whereas a single GSB peak with two ESA wings on two sides should be observed in metallic Au NCs (for the spherical case only, hence, requiring the knowledge of the NC shape<sup>57</sup> or X-ray structure<sup>35,50</sup>). Note that it is nontrivial to resolve the nonspherical or anisotropic shape of ultrasmall gold NCs of 1–3 nm. Nevertheless,  $\text{Au}_{333}$  was identified to be somewhat squashed, hence, two SPRs were seen in the TAS.<sup>57</sup> Therefore,

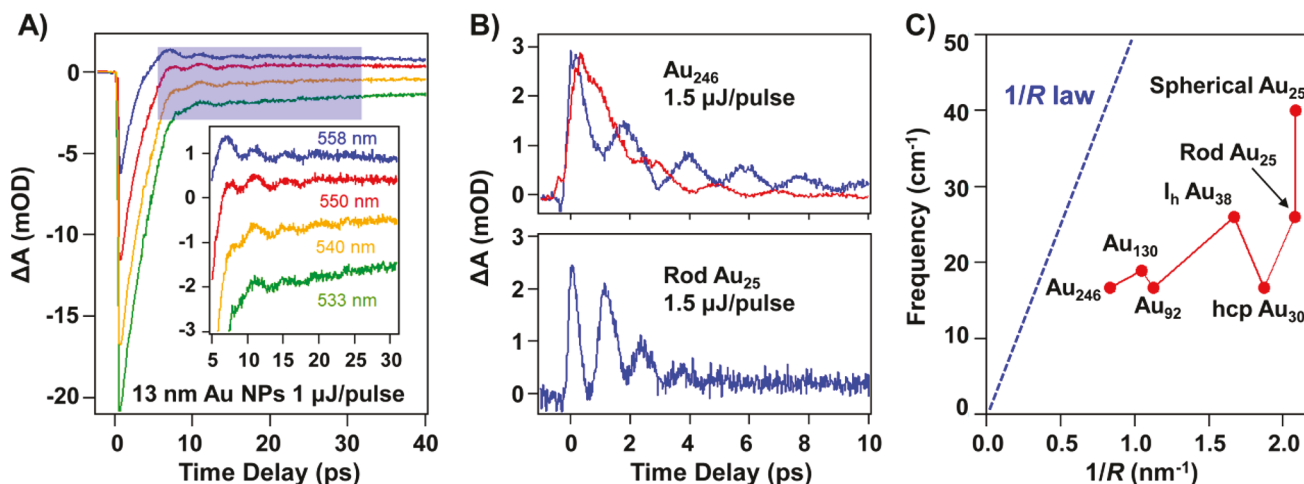


Figure 9. (A) Oscillations observed in the TA dynamics of 13 nm Au NPs (the inset shows the zoom-in of the oscillations). Reproduced under a Creative Commons CC-BY license from ref 67. Copyright 2019 MDPI. (B) Coherent oscillations observed in the TA dynamics of Au<sub>246</sub> and rod-shaped Au<sub>25</sub> NCs. Reproduced with permission from ref 34 (copyright 2017 Wiley-VCH) and reproduced from ref 68 (copyright 2011 American Chemical Society). (C) Oscillation frequency varying with 1/R of a series of Au NCs (the 1/R law for Au NPs is shown by a dashed blue line).

TAS is more powerful than steady-state absorption to differentiate molecular-like and metallic Au NCs.

**Excited-State Lifetime and Power Dependence.** The relaxation dynamics of excited states is also different between metallic-state and molecular-like Au NCs. In molecular-like Au NCs, photoexcitation gives rise to single-electron transition and the formation of excited states, which then experience an ultrafast cooling (<1 ps) to a lower excited state and finally return to the ground state.<sup>58</sup> The excited-state lifetimes of Au NCs ( $n < 100$ ,  $E_g > 0.5$  eV) are a few nanoseconds to microseconds.<sup>36,53</sup> As the size of Au NCs increases, the  $E_g$  will decrease accordingly, which will lead to shortening of the excited-state lifetime (Figure 7A).<sup>36</sup> In metallic Au NPs and NCs, which show negligible  $E_g$  after photoexcitation, collective excitation will heat up the electrons to a very high temperature (e.g., >1000 K).<sup>1,52,59,60</sup> The energy will be released from the electron to the lattice via electron–phonon coupling (typically 1–5 ps), and finally, the energy will be dissipated into the environment by phonon–phonon coupling (ph–ph coupling).<sup>21</sup> Therefore, molecular-like Au NCs show excited-state lifetimes longer than those of metallic Au NCs (few picoseconds). However, for those large Au NCs with  $k_B T$  level  $E_g$ , the excited-state lifetime decreases to a few picoseconds because of the diminishing  $E_g$  (Figure 7A).<sup>11,21,24,27,29,32</sup> which becomes comparable to that of the metallic state (Figure 7B). Therefore, comparing the excited-state lifetime cannot reliably determine the metallicity of large-sized Au NCs. Again, multiple analyses are required to reach the conclusion of metallic or nonmetallic state.

To further differentiate large-sized yet nonmetallic Au NCs and metallic ones, one needs a more effective strategy. In molecular-like Au NCs, relatively low carrier concentrations will give rise to suppressed Auger recombination, which makes the relaxation of the excited state less sensitive to pump power (Figure 8A).<sup>34</sup> In metallic Au NCs, the relaxation dynamics can be described by a two-temperature model:<sup>1</sup>

$$C_e(T_e) \frac{dT_e}{dt} = -g(T_e - T_l) \quad (2)$$

$$C_l \frac{dT_l}{dt} = g(T_e - T_l) \quad (3)$$

where  $T_e$  and  $T_l$  are the temperature of electrons and lattice, respectively,  $C_e$  and  $C_l$  are the heat capacity of electrons and lattice, respectively, and  $g$  is the electron–phonon coupling constant. Because  $C_e$  is dependent on the electron temperature, the e–p coupling is dependent on pump fluence and the excited-state dynamics is power-dependent (Figure 8B).<sup>35</sup> The pump power dependence of TA dynamics has been widely used to determine the metallicity of Au NCs. In 2002, Link *et al.* compared the relaxation dynamics of small Au NCs and plasmonic Au NPs and found that molecular-like Au NCs show power-independent dynamics.<sup>58</sup> In 2015, Mustalahti *et al.* reported power-independent mid-IR TA dynamics of Au<sub>102</sub> and Au<sub>130</sub> dynamics, which proved that both NCs are nonmetallic.<sup>24</sup> In 2016, Zhou *et al.* compared the power dependence of TA dynamics of a series Au NCs protected by the same type of ligand and mapped out the trend of e–p coupling versus the size (Figure 8C).<sup>21</sup> In 2018, Higaki *et al.* further observed that the nonmetal to metal transition occurs sharply between Au<sub>246</sub>(SR)<sub>80</sub> and Au<sub>279</sub>(SR)<sub>84</sub> using a similar method (Figure 8D).<sup>35</sup> To obtain accurate results, the power-dependent dynamics experiment needs to be performed within a linear power regime; that is, the initial TA signal intensity should increase linearly with the pump power so that the carrier density would not be too high to generate higher-order recombination.

Very recently, the photophysics of Au<sub>191</sub>(SR)<sub>66</sub> was reported, in which both multiple absorption peaks in the steady-state spectrum and power-dependent electron dynamics were observed.<sup>61</sup> In earlier work, both multiple GSB peaks and power-dependent electron dynamics were also reported for Au<sub>144</sub> and Au<sub>144-x</sub>Ag<sub>x</sub> NCs.<sup>27,62</sup> We believe that these three NCs should still be nonmetallic (at least Au<sub>144</sub> with  $E_g = 0.17$  eV),<sup>49</sup> but the origin of the power-dependent dynamics for these molecular-like Au NCs remains to be explained, and further experimental and theoretical studies are required. These cases also imply that multiple criteria should be applied to determine the metallicity of metal NCs between Au<sub>144</sub> and Au<sub>279</sub>.

Table 1. Criteria for Differentiating Metallic and Nonmetallic Au NCs and Distinct Features

criteria	metallic Au NCs	nonmetallic Au NCs	fidelity
definition	$E_g < k_B T$	$E_g > k_B T$	(theoretical)
optical absorption measurements of $E_g$		down to $\sim 0.5$ eV	medium
electrochemical measurements of $E_g$		down to $\sim 0.1$ eV (perhaps 0.05 eV)	high
UV-vis-NIR absorption	single peak (spherical particles)	multiple peaks (regardless of shape)	medium
cryogenic absorption	no sharpening	sharpening	high
TA spectra	single GSB peak (spherical particles)	multiple GSB peaks (regardless of shape)	medium
TA decay lifetime	1–5 ps (e–p coupling), 10–100 ps (ph–ph coupling)	several ps to $\mu$ s (dependent on size and structure)	low/medium
TA power dependence	yes	no	medium
TA oscillation frequency	1/R law, size-dependent	no 1/R law, structure-dependent	medium

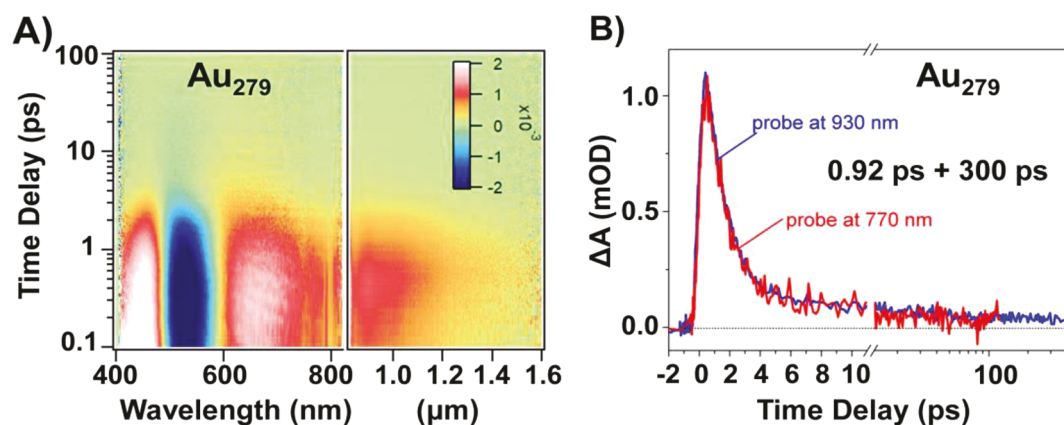


Figure 10. Photophysical properties of Au<sub>279</sub>. (A) UV-vis-NIR TA data map of Au<sub>279</sub> pumped at 370 nm. (B) Comparison of TA kinetic traces probed in visible and NIR ranges. Both panels are reprinted from ref 35. Copyright 2018 American Chemical Society.

**Coherent Oscillations in TA Dynamics.** In the TA dynamics of Au NCs and NPs, coherent oscillations are often observed when the laser pulse is short enough. In plasmonic Au NPs, collective photoexcitation of electrons will heat up the lattice, and the heating effect will cause the Au core to expand, which will cause the lattice vibration and accordingly a periodic shift of the SPR peak position.<sup>63</sup> Since the ultrashort laser can induce a rapid lattice heating and expansion ( $<100$  fs), it will impulsively excite the breathing modes because the lattice heating is much faster than the period of the vibrations.<sup>63</sup> Such a shift of the SPR peak caused by the breathing vibration will give rise to oscillations in the TA dynamics. In molecular-like Au NCs, following the single-electron photoexcitation, a wavepacket motion will be generated on the excited state, which will also be projected to the ground state *via* an impulsive stimulated Raman process.<sup>34,64,65</sup> Therefore, the oscillations in TA dynamics could originate from the wavepacket on both the excited state and the ground state, but the position of the phase shift can determine which one is detected.<sup>64,66</sup> The wavepacket motions will then be observed as oscillations in the TA dynamics as a result of e–p coupling. Not only are the origins of such oscillations different for molecular and metallic-state Au NCs, but also their behaviors are different. In metallic Au NPs and NCs, the oscillations are often observed on the two sides of the GSB peak, and the amplitude is relatively weak compared to the electron dynamics (Figure 9A).<sup>67</sup> In molecular-state Au NCs, oscillations could be observed over all the probe wavelengths, and the amplitudes of the oscillations are very strong in the initial few picoseconds compared to that of the electron dynamics (Figure 9B).<sup>34,68</sup> In other words, with a similar

carrier concentration (number of carriers in unit volume), oscillations in TA would be much easier to observe in nonmetallic Au NCs.

The phase and frequency information on coherent oscillations in Au NPs and NCs can be obtained by fitting the dynamics using a damped cosinusoidal function:<sup>34</sup>

$$\Delta A = e^{-t^2/2\sigma^2} \times [A_1 e^{-t/\tau_1} + A_2 e^{-t/\tau_2} + A_3 e^{-t/\tau_3} \cos(\omega t + \varphi)] \quad (4)$$

where  $\sigma$  is the standard deviation of Gaussian impulsive function,  $\tau_1$  and  $\tau_2$  are the TA relaxation time constants,  $\tau_3$  is the damping time of the oscillation,  $\omega$  is the frequency, and  $\varphi$  is the phase of the oscillation. It has been reported that the oscillation in Au NPs will show a phase shift on the two sides of the SPR peak.<sup>69</sup> On the other hand, oscillations in nonmetallic Au NCs will show a phase shift on the two sides of ESA or GSB depending on the origin of wavepacket motion.<sup>34,68</sup> Therefore, the phase shift of oscillation in TA dynamics can also be used to determine the metallicity of Au NCs.

In Au NPs, the oscillation originates from the acoustic vibration of the metal nanoparticle, and the frequency of the oscillation was found to be inversely proportional to the radius (denoted  $R$ ) of the particle ( $1/R$  law, Figure 9C).<sup>1</sup> In molecular-state Au NCs, the frequencies of the oscillation deviate from the  $1/R$  law of the plasmonic NPs (Figure 9C), which indicates that the continuum model is no longer valid for molecular-like Au NCs. One can observe that molecular-like Au NCs show oscillation frequencies below the  $1/R$  plot, and they are not strongly correlated with the size. Therefore,

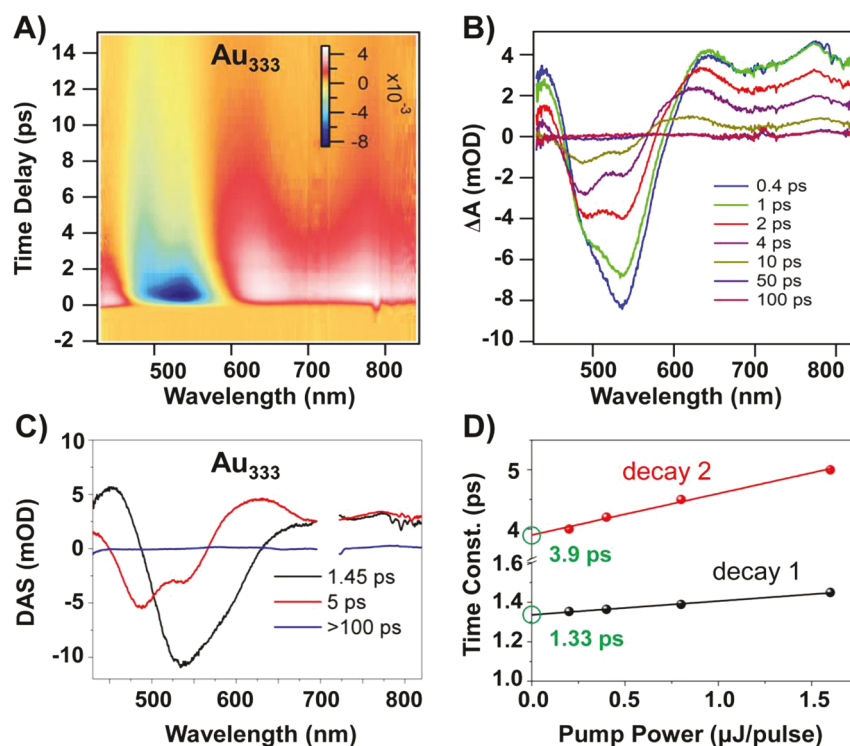


**Figure 11.** Photophysical properties of the Au<sub>333</sub> NC. (A) TA data map of Au<sub>333</sub> pumped at 360 nm. (B) TA spectra of Au<sub>333</sub> probed at different time delays. (C) Decay associated spectra and time constant obtained from global fitting of the data in (A). (D) Decay time constants as a function of pump laser power. Panels A–D are reprinted with permission from ref 57. Copyright 2019 National Academy of Sciences.

the structure rather than size plays a more significant role in the coherent vibration in these ultrasmall molecular-like Au NCs. By looking into the amplitude, phase shift, and frequency of the oscillation in TA, one would be able to differentiate metallic and nonmetallic Au NCs. Of note, Maioli *et al.* recently investigated the breathing modes of very small Au NCs and found that a  $1/R$  dependence of the breathing mode persists to very small sizes.<sup>70</sup> Further experimental and theoretical works are still required to deeply understand the coherent oscillations in Au NCs.

**Summary of Various Criteria.** In Table 1, the criteria discussed above are summarized, and the different behaviors of metallic and nonmetallic Au NCs are also listed. A single criterion or method may not be of high fidelity in differentiating the molecular *versus* metallic state; rather, by combining multiple testing methods and criteria, it becomes more reliable to analyze the metallicity in Au NCs.

### GOLD NANOCCLUSERS WITH NASCENT SURFACE PLASMON RESONANCE

Gold NCs with SPR are classified as metallic since an electron gas is formed at negligibly small  $E_g$ . Interestingly, those Au NCs with nascent SPR were reported to exhibit some different photophysical behaviors compared to those of their larger counterparts. In 2018, the electron dynamics of Au<sub>279</sub>, the smallest plasmonic Au NC, was reported.<sup>35,50</sup> UV–vis–NIR TA measurements on Au<sub>279</sub> revealed that there is a broad ESA shoulder in the NIR region (Figure 10A).<sup>35</sup> Similar broad ESA shoulders were also observed for Au<sub>333</sub>, Au<sub>~520</sub>, and Au<sub>~940</sub> NCs (Figure 6B) but not in larger plasmonic NPs.<sup>1,63</sup> Moreover, the intrinsic e–p coupling time of Au<sub>279</sub> is 0.92 ps, and the ph–ph coupling time is around 300 ps (Figure

10B). The  $\sim 1$  ps e–p coupling time is normal for Au<sub>279</sub>, while the 300 ps ph–ph coupling time is very long (ph–ph time is  $\sim 10$  ps for 4 nm Au NPs)<sup>71</sup> considering its small size and large surface-to-volume ratio. This observation makes the nascent SPR of Au<sub>279</sub> quite interesting in optical properties compared to larger-sized Au NPs. The origin of the unusual photophysical properties requires further experimental or theoretical work.

In another Au NC with nascent SPR, Au<sub>333</sub>(SR)<sub>79</sub> (Au<sub>333</sub> for short), we also observed interesting optical properties.<sup>57</sup> In the TA data, one can observe two GSB peaks around 540 and 485 nm (Figure 11A,B). Moreover, an additional dip on the ESA around 700 nm was also observed, which could be another GSB peak. The observation of multiple GSB peaks in Au<sub>333</sub> was also reflected in low-temperature steady-state absorption measurements. Global fitting of the TA data revealed three decay components, with the first two components both dependent on the pump fluence (Figure 11C,D). The first and second decay components have an intrinsic lifetime of 1.33 and 3.9 ps, respectively. The first decay component (1.33 ps) was assigned to the e–p coupling of Au<sub>333</sub>, while the second decay component (3.9 ps) and the third component were explained as the ph–ph coupling processes. Such an observation was partly ascribed to the oblate shape of Au<sub>333</sub>. The interesting photophysical properties of Au<sub>333</sub> will stimulate future studies on those Au NCs with nascent SPR.

### ESTIMATION OF ULTRASMALL ENERGY GAP BASED ON EXCITED STATE LIFETIME

The onset of steady-state absorption in large-size Au NCs (>100 gold atoms) lies in the NIR and even the IR region, thus it is challenging to determine so small gaps by optical/IR

measurements. Recent work by Zhou *et al.* showed that the excited-state lifetimes of Au NCs decrease exponentially with the energy gaps when  $E_g < 0.5$  eV (Figure 12A),<sup>35</sup> which may

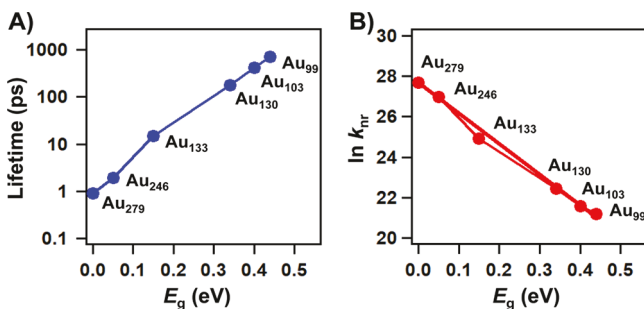


**Figure 12.** Correlation between the energy gaps and the excited-state lifetimes of Au NCs. (A) Excited-state lifetime versus  $E_g$  for large-size Au NCs; (B)  $\ln k_{nr}$  versus  $E_g$  for large-size Au NCs. Reproduced from ref 36. Copyright 2019 American Chemical Society.

serve as an estimation. Based on the energy gap law, the nonradiative recombination rate ( $k_{nr}$ ) of Au NCs can be expressed as<sup>31,35</sup>

$$k_{nr} = Ae^{-\gamma E_g/\hbar\omega} \quad (5)$$

where  $\gamma$  is the molecular parameter and  $\omega$  is the highest vibrational frequency involved in the nonradiative decay. For large-size Au NCs, their relaxation dynamics is dominated by nonradiative decay, and  $k_{nr}$  can be calculated based on the excited-state lifetime obtained from TA measurements. The  $\ln k_{nr}$  and  $E_g$  plot exhibit a good linear relationship (Figure 12B). By measuring the average excited-state lifetime and calculating the nonradiative recombination rate, one could estimate the  $E_g$  of large-sized Au NCs using the following equation:

$$\ln k_{nr} = \ln A - \frac{\gamma}{\hbar\omega} E_g \quad (6)$$

In Figure 12B, the fitted intercept ( $\ln A$ ) is 27.7 and the gradient ( $-\gamma/\hbar\omega$ ) is  $-15.1$  eV<sup>-1</sup>. For Au<sub>279</sub>,  $E_g$  is negligibly small and could be taken as zero, and the e-p coupling time was reported to be 0.92 ps.<sup>35</sup> If we view the e-p coupling rate as the nonradiative recombination rate,  $k_{nr} = 1.07 \times 10^{12}$  s<sup>-1</sup>, that is,  $\ln k_{nr} = 27.7$ , which matches well with the fitted intercept value. Therefore, the excited-state recombination lifetime measured by TA spectroscopy could be used to estimate the energy gap of large-sized Au NCs ( $n > 100$ ).

## CONCLUSION AND FUTURE PERSPECTIVE

The size-induced transition from a metallic to a nonmetallic state has been pursued for many decades, including in both theoretical and experimental work.<sup>72–84</sup> For the latter, a prerequisite is to prepare a series of sizes (“snapshots” of the size evolution), and it is also critical to solve the atomic structures of those sizes (*e.g.*, their shape, symmetry, surface ligands, and metal-ligand bonding modes) for correlating with the spectroscopic results, but all of these were very daunting tasks until the recent establishment of atomically precise nanochemistry. With the great advances achieved in recent years, it is now possible to investigate the decades-long fundamental question through the structure–property correlation, albeit it is still not an easy task.

Using atomically precise Au NCs as a model system, we have discussed the distinct behaviors of the metallic state *versus* the molecular (or nonmetallic) state. The criteria to determine the metallicity of Au NCs include (1)  $E_g$  determined by optical and electrochemical methods (unfortunately,  $E_g$  below 0.1 eV is difficult to measure reliably, which calls for other analyses); (2) steady-state UV–vis–NIR absorption spectra; (3) cryogenic absorption spectra; (4) TA spectra; (5) TA lifetime and dynamics power dependence; and (6) TA oscillation phase and frequency. The major difficulty is the determination of ultrasmall  $E_g$  on the order of meV or  $k_B T$  for large-sized Au NCs, for which we have proposed a method to estimate the ultrasmall energy gaps based on the excited-state lifetimes of NCs. These criteria are of major importance to understand the metallic to molecular state transition in Au and other metal NCs. The interesting photophysical properties of Au NCs with nascent SPR are also discussed, which will stimulate future experimental and theoretical studies on the properties and applications of Au NCs, in particular, those in the metal to nonmetal transition regime.

The sharp transition from Au<sub>246</sub> to Au<sub>279</sub> came as a surprise, and it implies that the simple theory’s prediction of  $E_g$  versus  $1/n$  (where  $n$  is the number of metal atoms) is insufficient as this relation cannot explain such an abrupt transition. This simple relation does not take into consideration any structural effect of the metal core nor the electron correlation effect. X-ray crystallography revealed that Au<sub>246</sub> has a decahedral structure, whereas Au<sub>279</sub> is face-centered cubic; thus, one may argue that the potential structural influence might be in operation. Future work should synthesize more Au<sub>*n*</sub>(SR)<sub>*m*</sub> sizes in the transition region and carry out careful investigations to address the issues.

So far the vast majority of the reported Au<sub>*n*</sub>(SR)<sub>*m*</sub> structures are quasi-spherical, especially those large sizes (including Au<sub>246</sub> and Au<sub>279</sub>). The influence of particle shape<sup>82–84</sup> (*e.g.*, one-dimensional rods and two-dimensional oblate structures) on the nonmetal to metal transition remains unclear. In the metallic/plasmonic regime, the shape effects are apparently significant, but to what extent the shape influences the transition in the quantum size regime remains to be mapped out in future work.

The ligand factor is also of interest. While the majority of reported NCs are protected by thiolate ligands, there have been extensions to other types of ligands<sup>16,85</sup> such as alkynyl and mixed ligands on the NCs. Future work will find out more details of the ligand influence on the nonmetal to metal transition. Related to the ligand factor, bare NCs without ligand protection are also worthy of a comparison in future research, though achieving large bare NCs and determining their electronic and optical properties are certainly challenging.

Finally, an extension from the gold system to other metals including Ag, Cu, Pd, Pt, and alloy systems is also suggested for future work, especially the synergism in alloys deserves much effort. Different metals exhibit distinct differences in electron exchange and correlation effects, spin–orbit coupling, electronic polarizability and other aspects. Thus, the extension will certainly find out more fundamental details about the emergence of metallic state and the nature of the metallic bond. Understanding such fundamentals will greatly benefit the design of functional materials for specific applications.

## AUTHOR INFORMATION

## Corresponding Authors

Rongchao Jin – Department of Chemistry, Carnegie Mellon University, Pittsburgh, Pennsylvania 15213, United States; [orcid.org/0000-0002-2525-8345](https://orcid.org/0000-0002-2525-8345); Email: [rongchao@andrew.cmu.edu](mailto:rongchao@andrew.cmu.edu)

He Wang – Department of Physics, University of Miami, Coral Gables, Florida 33146, United States; [orcid.org/0000-0003-1365-0304](https://orcid.org/0000-0003-1365-0304); Email: [hewang@miami.edu](mailto:hewang@miami.edu)

## Authors

Meng Zhou – Department of Chemistry, Carnegie Mellon University, Pittsburgh, Pennsylvania 15213, United States; Department of Physics, University of Miami, Coral Gables, Florida 33146, United States; [orcid.org/0000-0001-5187-9084](https://orcid.org/0000-0001-5187-9084)

Xiangsha Du – Department of Chemistry, Carnegie Mellon University, Pittsburgh, Pennsylvania 15213, United States

Complete contact information is available at:

<https://pubs.acs.org/10.1021/acsnano.1c04705>

## Notes

The authors declare no competing financial interest.

## ACKNOWLEDGMENTS

R.J. acknowledges the financial support from the National Science Foundation (NSF DMR-1808675); M.Z. and H.W. acknowledge the financial support by the Air Force Office of Scientific Research (AFOSR) Award No. FA9550-17-1-0099.

## VOCABULARY

**Nanoclusters**, atomically precise particles with definitive formulas; **nonmetallic state**, the electronic structure being composed of discrete states with an appreciable gap between energy levels; **metallic state**, defined as the zero gap state for bulk materials, but for a finite system (such as nanoclusters), a theoretical definition is when the energy gap is smaller than  $k_B T$ ; **optical gap**, when the optical absorbance is extrapolated to zero, the intercept with the photon wavelength (or energy) is taken as the optical gap, which equals to the HOMO–LUMO gap in the case of dipole-allowed electronic excitation; **electrochemical gap**, unlike the optical gap the electrochemical gap is not subjected to the dipole selection rule, but the resolution in measurements is affected by the thermal energy and the specific method as well as the fluctuations in charging energy

## REFERENCES

(1) Hartland, G. V. Optical Studies of Dynamics in Noble Metal Nanostructures. *Chem. Rev.* **2011**, *111*, 3858–87.  
(2) Abb, M.; Wang, Y.; de Groot, C. H.; Muskens, O. L. Hotspot-Mediated Ultrafast Nonlinear Control of Multifrequency Plasmonic Nanoantennas. *Nat. Commun.* **2014**, *5*, 4869.  
(3) Brongersma, M. L.; Halas, N. J.; Nordlander, P. Plasmon-Induced Hot Carrier Science and Technology. *Nat. Nanotechnol.* **2015**, *10*, 25–34.  
(4) Wu, K.; Chen, J.; McBride, J. R.; Lian, T. Efficient Hot-Electron Transfer by a Plasmon-Induced Interfacial Charge-Transfer Transition. *Science* **2015**, *349*, 632–635.  
(5) Dawson, A.; Kamat, P. V. Semiconductor–Metal Nano-composites. Photoinduced Fusion and Photocatalysis of Gold-Capped TiO<sub>2</sub> (TiO<sub>2</sub>/Gold) Nanoparticles. *J. Phys. Chem. B* **2001**, *105*, 960–966.

(6) Cao, Y. C.; Jin, R.; Mirkin, C. A. Nanoparticles with Raman Spectroscopic Fingerprints for DNA and RNA Detection. *Science* **2002**, *297*, 1536–1540.

(7) Zhu, M.; Aikens, C. M.; Hollander, F. J.; Schatz, G. C.; Jin, R. Correlating the Crystal Structure of a Thiol-Protected Au<sub>25</sub> Cluster and Optical Properties. *J. Am. Chem. Soc.* **2008**, *130*, 5883–5885.

(8) Jin, R.; Zeng, C.; Zhou, M.; Chen, Y. Atomically Precise Colloidal Metal Nanoclusters and Nanoparticles: Fundamentals and Opportunities. *Chem. Rev.* **2016**, *116*, 10346–413.

(9) Zeng, C.; Chen, Y.; Kirschbaum, K.; Lambright, K. J.; Jin, R. Emergence of Hierarchical Structural Complexities in Nanoparticles and Their Assembly. *Science* **2016**, *354*, 1580–1584.

(10) Yang, S.; Chen, S.; Xiong, L.; Liu, C.; Yu, H.; Wang, S.; Rosi, N. L.; Pei, Y.; Zhu, M. Total Structure Determination of Au<sub>16</sub>(S-Adm)<sub>12</sub> and Cd<sub>1</sub>Au<sub>14</sub>(StBu)<sub>12</sub> and Implications for the Structure of Au<sub>15</sub>(SR)<sub>13</sub>. *J. Am. Chem. Soc.* **2018**, *140*, 10988–10994.

(11) Zeng, C.; Chen, Y.; Kirschbaum, K.; Appavoo, K.; Sfeir, M. Y.; Jin, R. Structural Patterns at All Scales in a Nonmetallic Chiral Au<sub>133</sub>(SR)<sub>52</sub> Nanoparticle. *Sci. Adv.* **2015**, *1*, No. e1500045.

(12) Aikens, C. M. Electronic and Geometric Structure, Optical Properties, and Excited State Behavior in Atomically Precise Thiolate-Stabilized Noble Metal Nanoclusters. *Acc. Chem. Res.* **2018**, *51*, 3065–3073.

(13) Gan, Z.; Xia, N.; Wu, Z. Discovery, Mechanism, and Application of Antigalvanic Reaction. *Acc. Chem. Res.* **2018**, *51*, 2774–2783.

(14) Ghosh, A.; Mohammed, O. F.; Bakr, O. M. Atomic-Level Doping of Metal Clusters. *Acc. Chem. Res.* **2018**, *51*, 3094–3103.

(15) Kwak, K.; Lee, D. Electrochemistry of Atomically Precise Metal Nanoclusters. *Acc. Chem. Res.* **2019**, *52*, 12–22.

(16) Lei, Z.; Wan, X.-K.; Yuan, S.-F.; Guan, Z.-J.; Wang, Q.-M. Alkynyl Approach toward the Protection of Metal Nanoclusters. *Acc. Chem. Res.* **2018**, *51*, 2465–2474.

(17) Wang, S.; Li, Q.; Kang, X.; Zhu, M. Customizing the Structure, Composition, and Properties of Alloy Nanoclusters by Metal Exchange. *Acc. Chem. Res.* **2018**, *51*, 2784–2792.

(18) Yao, Q.; Chen, T.; Yuan, X.; Xie, J. Toward Total Synthesis of Thiolate-Protected Metal Nanoclusters. *Acc. Chem. Res.* **2018**, *51*, 1338–1348.

(19) Yau, S. H.; Varnavski, O.; Goodson, T. An Ultrafast Look at Au Nanoclusters. *Acc. Chem. Res.* **2013**, *46*, 1506–1516.

(20) Abbas, M. A.; Kamat, P. V.; Bang, J. H. Thiolated Gold Nanoclusters for Light Energy Conversion. *ACS Energy Lett.* **2018**, *3*, 840–854.

(21) Zhou, M.; Zeng, C.; Chen, Y.; Zhao, S.; Sfeir, M. Y.; Zhu, M.; Jin, R. Evolution from the Plasmon to Exciton State in Ligand-Protected Atomically Precise Gold Nanoparticles. *Nat. Commun.* **2016**, *7*, 13240.

(22) Malola, S.; Lehtovaara, L.; Enkovaara, J.; Häkkinen, H. Birth of the Localized Surface Plasmon Resonance in Monolayer-Protected Gold Nanoclusters. *ACS Nano* **2013**, *7*, 10263–10270.

(23) Iida, K.; Noda, M.; Nobusada, K. Interface Electronic Properties between a Gold Core and Thiolate Ligands: Effects on an Optical Absorption Spectrum in Au<sub>133</sub>(SPh<sup>t</sup>Bu)<sub>52</sub>. *J. Phys. Chem. C* **2016**, *120*, 2753–2759.

(24) Mustalahti, S.; Myllyperkiö, P.; Lahtinen, T.; Malola, S.; Salorinne, K.; Tero, T.-R.; Koivisto, J.; Häkkinen, H.; Pettersson, M. Photodynamics of a Molecular Water-Soluble Nanocluster Identified as Au<sub>130</sub>(pMBA)<sub>50</sub>. *J. Phys. Chem. C* **2015**, *119*, 20224–20229.

(25) Knoppe, S.; Verbiest, T. Resonance Enhancement of Nonlinear Optical Scattering in Monolayer-Protected Gold Clusters. *J. Am. Chem. Soc.* **2017**, *139*, 14853–14856.

(26) Yi, C.; Zheng, H.; Tvedte, L. M.; Ackerson, C. J.; Knappenberger, K. L. Nanometals: Identifying the Onset of Metallic Relaxation Dynamics in Monolayer-Protected Gold Clusters Using Femtosecond Spectroscopy. *J. Phys. Chem. C* **2015**, *119*, 6307–6313.

(27) Yi, C.; Tofanelli, M. A.; Ackerson, C. J.; Knappenberger, K. L. Optical Properties and Electronic Energy Relaxation of Metallic

- Au<sub>144</sub>(SR)<sub>60</sub> Nanoclusters. *J. Am. Chem. Soc.* **2013**, *135*, 18222–18228.
- (28) Maity, S.; Bain, D.; Patra, A. An Overview on the Current Understanding of the Photophysical Properties of Metal Nanoclusters and Their Potential Applications. *Nanoscale* **2019**, *11*, 22685–22723.
- (29) Varnavski, O.; Ramakrishna, G.; Kim, J.; Lee, D.; Goodson, T. Critical Size for the Observation of Quantum Confinement in Optically Excited Gold Clusters. *J. Am. Chem. Soc.* **2010**, *132*, 16–17.
- (30) Philip, R.; Chantharasupawong, P.; Qian, H.; Jin, R.; Thomas, J. Evolution of Nonlinear Optical Properties: From Gold Atomic Clusters to Plasmonic Nanocrystals. *Nano Lett.* **2012**, *12*, 4661–4667.
- (31) Negishi, Y.; Nakazaki, T.; Malola, S.; Takano, S.; Niihori, Y.; Kurashige, W.; Yamazoe, S.; Tsukuda, T.; Häkkinen, H. A Critical Size for Emergence of Nonbulk Electronic and Geometric Structures in Dodecanethiolate-Protected Au Clusters. *J. Am. Chem. Soc.* **2015**, *137*, 1206–1212.
- (32) Kwak, K.; Thanthirige, V. D.; Pyo, K.; Lee, D.; Ramakrishna, G. Energy Gap Law for Exciton Dynamics in Gold Cluster Molecules. *J. Phys. Chem. Lett.* **2017**, *8*, 4898–4905.
- (33) Mustalahti, S.; Myllyperkiö, P.; Lahtinen, T.; Salorinne, K.; Malola, S.; Koivisto, J.; Häkkinen, H.; Pettersson, M. Ultrafast Electronic Relaxation and Vibrational Cooling Dynamics of Au<sub>144</sub>(SC<sub>2</sub>H<sub>4</sub>Ph)<sub>60</sub> Nanocluster Probed by Transient Mid-IR Spectroscopy. *J. Phys. Chem. C* **2014**, *118*, 18233–18239.
- (34) Zhou, M.; Zeng, C.; Song, Y.; Padelford, J. W.; Wang, G.; Sfeir, M. Y.; Higaki, T.; Jin, R. On the Non-Metallicity of 2.2 nm Au<sub>246</sub>(SR)<sub>80</sub> Nanoclusters. *Angew. Chem., Int. Ed.* **2017**, *56*, 16257–16261.
- (35) Higaki, T.; Zhou, M.; Lambright, K. J.; Kirschbaum, K.; Sfeir, M. Y.; Jin, R. Sharp Transition from Nonmetallic Au<sub>246</sub> to Metallic Au<sub>279</sub> with Nascent Surface Plasmon Resonance. *J. Am. Chem. Soc.* **2018**, *140*, 5691–5695.
- (36) Zhou, M.; Higaki, T.; Li, Y.; Zeng, C.; Li, Q.; Sfeir, M. Y.; Jin, R. Three-Stage Evolution from Non-scalable to Scalable Optical Properties of Thiolate-Protected Gold Nanoclusters. *J. Am. Chem. Soc.* **2019**, *141*, 19754–19764.
- (37) Qian, H.; Jiang, D.-e.; Li, G.; Gayathri, C.; Das, A.; Gil, R. R.; Jin, R. Monoplatinum Doping of Gold Nanoclusters and Catalytic Application. *J. Am. Chem. Soc.* **2012**, *134*, 16159–16162.
- (38) Higaki, T.; Liu, C.; Zhou, M.; Luo, T. Y.; Rosi, N. L.; Jin, R. Tailoring the Structure of 58-Electron Gold Nanoclusters: Au<sub>103</sub>S<sub>2</sub>(S-Nap)<sub>41</sub> and Its Implications. *J. Am. Chem. Soc.* **2017**, *139*, 9994–10001.
- (39) Weissker, H. C.; Escobar, H. B.; Thanthirige, V. D.; Kwak, K.; Lee, D.; Ramakrishna, G.; Whetten, R. L.; López-Lozano, X. Information on Quantum States Pervades the Visible Spectrum of the Ubiquitous Au<sub>144</sub>(SR)<sub>60</sub> Gold Nanocluster. *Nat. Commun.* **2014**, *5*, 3785.
- (40) Chen, Y.; Zeng, C.; Kauffman, D. R.; Jin, R. Tuning the Magic Size of Atomically Precise Gold Nanoclusters via Isomeric Methylbenzenethiols. *Nano Lett.* **2015**, *15*, 3603–3609.
- (41) Li, G.; Zeng, C.; Jin, R. Thermally Robust Au<sub>99</sub>(SPh)<sub>42</sub> Nanoclusters for Chemoselective Hydrogenation of Nitrobenzaldehyde Derivatives in Water. *J. Am. Chem. Soc.* **2014**, *136*, 3673–3679.
- (42) Hulkko, E.; Lopez-Acevedo, O.; Koivisto, J.; Levi-Kalishman, Y.; Kornberg, R. D.; Pettersson, M.; Häkkinen, H. Electronic and Vibrational Signatures of the Au<sub>102</sub>(p-MBA)<sub>44</sub> Cluster. *J. Am. Chem. Soc.* **2011**, *133*, 3752–3755.
- (43) Zhou, M.; Yao, C.; Sfeir, M. Y.; Higaki, T.; Wu, Z.; Jin, R. Excited-State Behaviors of M<sub>1</sub>Au<sub>24</sub>(SR)<sub>18</sub> Nanoclusters: The Number of Valence Electrons Matters. *J. Phys. Chem. C* **2018**, *122*, 13435–13442.
- (44) Murray, R. W. Nanoelectrochemistry: Metal Nanoparticles, Nanoelectrodes, and Nanopores. *Chem. Rev.* **2008**, *108*, 2688–2720.
- (45) Antonello, S.; Perera, N. V.; Ruzzi, M.; Gascón, J. A.; Maran, F. Interplay of Charge State, Lability, and Magnetism in the Molecule-like Au<sub>25</sub>(SR)<sub>18</sub> Cluster. *J. Am. Chem. Soc.* **2013**, *135*, 15585–15594.
- (46) Wang, D.; Padelford, J. W.; Ahuja, T.; Wang, G. Transitions in Discrete Absorption Bands of Au<sub>130</sub> Clusters upon Stepwise Charging by Spectroelectrochemistry. *ACS Nano* **2015**, *9*, 8344–8351.
- (47) Padelford, J. W.; Zhou, M.; Chen, Y.; Jin, R.; Wang, G. Electronic Transitions in Highly Symmetric Au<sub>130</sub> Nanoclusters by Spectroelectrochemistry and Ultrafast Spectroscopy. *J. Phys. Chem. C* **2017**, *121*, 21217–21224.
- (48) Qian, H.; Jin, R. Ambient Synthesis of Au<sub>144</sub>(SR)<sub>60</sub> Nanoclusters in Methanol. *Chem. Mater.* **2011**, *23*, 2209–2217.
- (49) Chen, S.; Higaki, T.; Ma, H.; Zhu, M.; Jin, R.; Wang, G. Inhomogeneous Quantized Single-Electron Charging and Electrochemical–Optical Insights on Transition-Sized Atomically Precise Gold Nanoclusters. *ACS Nano* **2020**, *14*, 16781–16790.
- (50) Sakthivel, N. A.; Stener, M.; Sementa, L.; Fortunelli, A.; Ramakrishna, G.; Dass, A. Au<sub>279</sub>(SR)<sub>84</sub>: The Smallest Gold Thiolate Nanocrystal That Is Metallic and the Birth of Plasmon. *J. Phys. Chem. Lett.* **2018**, *9*, 1295–1300.
- (51) Devadas, M. S.; Bairu, S.; Qian, H.; Sinn, E.; Jin, R.; Ramakrishna, G. Temperature-Dependent Optical Absorption Properties of Monolayer-Protected Au<sub>25</sub> and Au<sub>38</sub> Clusters. *J. Phys. Chem. Lett.* **2011**, *2*, 2752–2758.
- (52) Link, S.; El-Sayed, M. A. Size and Temperature Dependence of the Plasmon Absorption of Colloidal Gold Nanoparticles. *J. Phys. Chem. B* **1999**, *103*, 4212–4217.
- (53) Zhou, M.; Higaki, T.; Hu, G.; Sfeir, M. Y.; Chen, Y.; Jiang, D.-e.; Jin, R. Three-Orders-of-Magnitude Variation of Carrier Lifetimes with Crystal Phase of Gold Nanoclusters. *Science* **2019**, *364*, 279–282.
- (54) Thanthirige, V. D.; Kim, M.; Choi, W.; Kwak, K.; Lee, D.; Ramakrishna, G. Temperature-Dependent Absorption and Ultrafast Exciton Relaxation Dynamics in MAu<sub>24</sub>(SR)<sub>18</sub> Clusters (M = Pt, Hg): Role of the Central Metal Atom. *J. Phys. Chem. C* **2016**, *120*, 23180–23188.
- (55) Stampelcoskie, K. G.; Kamat, P. V. Size-Dependent Excited State Behavior of Glutathione-Capped Gold Clusters and Their Light-Harvesting Capacity. *J. Am. Chem. Soc.* **2014**, *136*, 11093–11099.
- (56) Zhou, M.; Zeng, C.; Sfeir, M. Y.; Cotlet, M.; Iida, K.; Nobusada, K.; Jin, R. Evolution of Excited-State Dynamics in Periodic Au<sub>28</sub>, Au<sub>36</sub>, Au<sub>44</sub>, and Au<sub>52</sub> Nanoclusters. *J. Phys. Chem. Lett.* **2017**, *8*, 4023–4030.
- (57) Higaki, T.; Zhou, M.; He, G.; House, S. D.; Sfeir, M. Y.; Yang, J. C.; Jin, R. Anomalous Phonon Relaxation in Au<sub>333</sub>(SR)<sub>79</sub> Nanoparticles with Nascent Plasmons. *Proc. Natl. Acad. Sci. U. S. A.* **2019**, *116*, 13215–13220.
- (58) Link, S.; El-Sayed, M. A.; Schaaff, T. G.; Whetten, R. L. Transition from Nanoparticle to Molecular Behavior: A Femtosecond Transient Absorption Study of a Size-Selected 28 Atom Gold Cluster. *Chem. Phys. Lett.* **2002**, *356*, 240–246.
- (59) Hodak, J. H.; Henglein, A.; Hartland, G. V. Electron-Phonon Coupling Dynamics in Very Small (Between 2 and 8 nm Diameter) Au Nanoparticles. *J. Chem. Phys.* **2000**, *112*, 5942–5947.
- (60) Link, S.; El-Sayed, M. A. Spectral Properties and Relaxation Dynamics of Surface Plasmon Electronic Oscillations in Gold and Silver Nanodots and Nanorods. *J. Phys. Chem. B* **1999**, *103*, 8410–8426.
- (61) Sakthivel, N. A.; Shabaninezhad, M.; Sementa, L.; Yoon, B.; Stener, M.; Whetten, R. L.; Ramakrishna, G.; Fortunelli, A.; Landman, U.; Dass, A. The Missing Link: Au<sub>191</sub>(SPh-tBu)<sub>66</sub> Janus Nanoparticle with Molecular and Bulk-Metal-like Properties. *J. Am. Chem. Soc.* **2020**, *142*, 15799–15814.
- (62) Zheng, H.; Tofanelli, M. A.; Ackerson, C. J.; Knappenberger, K. L. Composition-Dependent Electronic Energy Relaxation Dynamics of Metal Domains as Revealed by Bimetallic Au<sub>144-x</sub>Ag<sub>x</sub>(SC<sub>8</sub>H<sub>9</sub>)<sub>60</sub> Monolayer-Protected Clusters. *Phys. Chem. Chem. Phys.* **2017**, *19*, 14471–14477.
- (63) Hartland, G. V. Coherent Excitation of Vibrational Modes in Metallic Nanoparticles. *Annu. Rev. Phys. Chem.* **2006**, *57*, 403–430.
- (64) Rafiq, S.; Scholes, G. D. Slow Intramolecular Vibrational Relaxation Leads to Long-Lived Excited-State Wavepackets. *J. Phys. Chem. A* **2016**, *120*, 6792–6799.

(65) Bardeen, C. J.; Wang, Q.; Shank, C. V. Selective Excitation of Vibrational Wave Packet Motion Using Chirped Pulses. *Phys. Rev. Lett.* **1995**, *75*, 3410–3413.

(66) Zhou, M.; Jin, R. Optical Properties and Excited-State Dynamics of Atomically Precise Gold Nanoclusters. *Annu. Rev. Phys. Chem.* **2021**, *72*, 121–142.

(67) Zhou, M.; Zeng, C.; Li, Q.; Higaki, T.; Jin, R. Gold Nanoclusters: Bridging Gold Complexes and Plasmonic Nanoparticles in Photophysical Properties. *Nanomaterials* **2019**, *9*, 933.

(68) Sfeir, M. Y.; Qian, H.; Nobusada, K.; Jin, R. Ultrafast Relaxation Dynamics of Rod-Shaped 25-Atom Gold Nanoclusters. *J. Phys. Chem. C* **2011**, *115*, 6200–6207.

(69) Hartland, G. V. Coherent Vibrational Motion in Metal Particles: Determination of the Vibrational Amplitude and Excitation Mechanism. *J. Chem. Phys.* **2002**, *116*, 8048–8055.

(70) Maioli, P.; Stoll, T.; Saucedo, H. E.; Valencia, I.; Demessence, A.; Bertorelle, F.; Crut, A.; Vallée, F.; Garzón, I. L.; Cerullo, G.; Del Fatti, N. Mechanical Vibrations of Atomically Defined Metal Clusters: From Nano- to Molecular-Size Oscillators. *Nano Lett.* **2018**, *18*, 6842–6849.

(71) Hu, M.; Hartland, G. V. Heat Dissipation for Au Particles in Aqueous Solution: Relaxation Time *versus* Size. *J. Phys. Chem. B* **2002**, *106*, 7029–7033.

(72) Kubo, R.; Kawabata, A.; Kobayashi, S. Electronic Properties of Small Particles. *Annu. Rev. Mater. Sci.* **1984**, *14*, 49–66.

(73) Zhang, H.; Hartmann, U.; Schmid, G. Energy-Level Splitting of Ligand-Stabilized Au<sub>55</sub> Clusters Observed by Scanning Tunneling Spectroscopy. *Appl. Phys. Lett.* **2004**, *84*, 1543.

(74) Kreibitz, U.; Vollmer, M. *Optical Properties of Metal Clusters*; Springer-Verlag: New York, 1995.

(75) Benfield, R. E. Mean Coordination Numbers and the Non-Metal-Metal Transition in Clusters. *J. Chem. Soc., Faraday Trans.* **1992**, *88*, 1107–1110.

(76) Mulder, F. M.; Thiel, R. C.; de Jongh, L. J.; Gubbens, P. C. M. Size-Evolution towards Metallic Behavior in Nano-Sized Gold and Platinum Clusters as Revealed by <sup>197</sup>Au Mössbauer Spectroscopy. *Nanostruct. Mater.* **1996**, *7*, 269–292.

(77) Johnston, R. L.; Rao, C. N. R.; Edwards, P. P. The Development of Metallic Behaviour in Clusters [and Discussion]. *Philos. Trans. R. Soc., A* **1998**, *356*, 211–230.

(78) Rao, C. N. R.; Kulkarni, G. U.; Thomas, P. J.; Edwards, P. P. Size-Dependent Chemistry: Properties of Nanocrystals. *Chem. - Eur. J.* **2002**, *8*, 28–35.

(79) von Issendorff, B.; Cheshnovsky, O. Metal to Insulator Transitions in Clusters. *Annu. Rev. Phys. Chem.* **2005**, *56*, 549–580.

(80) Li, J.; Li, X.; Zhai, H. J.; Wang, L. S. Au<sub>20</sub>: A Tetrahedral Cluster. *Science* **2003**, *299*, 864–867.

(81) Moseler, M.; Häkkinen, H.; Barnett, R. N.; Landman, U. Structure and Magnetism of Neutral and Anionic Palladium Clusters. *Phys. Rev. Lett.* **2001**, *86*, 2545–2548.

(82) Xu, W. W.; Li, Y.; Gao, Y.; Zeng, X. C. Unraveling a Generic Growth Pattern in Structure Evolution of Thiolate-Protected Gold Nanoclusters. *Nanoscale* **2016**, *8*, 7396–7401.

(83) Ma, Z.; Wang, P.; Pei, Y. Geometric Structure, Electronic Structure And Optical Absorption Properties of One-Dimensional Thiolate-Protected Gold Clusters Containing a Quasi-Face-Centered-Cubic (Quasi-Fcc) Au-Core: A Density-Functional Theoretical Study. *Nanoscale* **2016**, *8*, 17044–17054.

(84) Jiang, D.; Nobusada, K.; Luo, W.; Whetten, R. L. Thiolated Gold Nanowires: Metallic *versus* Semiconducting. *ACS Nano* **2009**, *3*, 2351–2357.

(85) Kenzler, S.; Schrenk, C.; Schnepf, A. Au<sub>108</sub>S<sub>24</sub>(PPh<sub>3</sub>)<sub>16</sub>: A Highly Symmetric Nanoscale Gold Cluster Confirms the General Concept of Metalloid Clusters. *Angew. Chem., Int. Ed.* **2017**, *56*, 393–396.